Localized in-gap state in a single-electron doped Mott insulator

Weng-Hang Leong,[1] Shun-Li Yu,[1] T. Xiang,[2,3] and Jian-Xin Li[1,4]

[1]*Department of Physics and National Laboratory of Solid State Microstructure, Nanjing University, Nanjing 210093, China*

[2]*Institute of Physics, Chinese Academy of Sciences, P.O. Box 603, Beijing 100190, China*

[3]*Collaborative Innovation Center of Quantum Matter, Beijing, China*

[4]*Collaborative Innovation Center of Advanced Microstructures, Nanjing University, Nanjing 210093, China*

(Received 11 February 2014; revised manuscript received 30 September 2014; published 1 December 2014)

Motivated by the recent atomic-scale scanning tunneling microscope (STM) observation for a spatially localized in-gap state in an electron doped Mott insulator, we evaluate the local electronic state of the Hubbard model on the square lattice using the cluster perturbation theory. An in-gap state is found to exist below the upper Hubbard band around the dopant lattice site, which is consistent with the STM measurements. The emergence of this local in-gap state is accompanied with a rapid reduction of the double occupancy of electrons. A similar in-gap state is also found to exist on the triangular lattice. These results suggest that the in-gap state is an inherent feature of Mott insulators independent of the lattice structure.

DOI: 10.1103/PhysRevB.90.245102 PACS number(s): 74.72.Cj, 71.10.Fd, 71.27.+a

I. INTRODUCTION

The mechanism underlying high-T_c superconductivity in cuprates remains one of the most challenging and fundamental problems in condensed matter physics [1]. All cuprate superconductors have a layered structure made up of one or more CuO_2 planes. Their parent compounds have one unpaired electron per Cu unit cell, which constitutes a Mott insulating ground state with an antiferromagnetic (AF) long range order [2]. By doping holes or electrons to CuO_2 planes, the AF order is suppressed and a superconducting phase emerges above a critical doping concentration. The evolution from the AF Mott insulating phase to the superconducting phase induced by doping is highly nontrivial [1]. A thorough investigation on the charge and spin dynamics of doped Mott insulators is believed to be the key for the understanding of extraordinary phenomena observed in high-T_c superconductors, such as the pseudogap effect.

The dynamics of a single hole in an antiferromagnetic Mott insulator has been extensively studied using the self-consistent Born approximation [3–8], finite-size exact diagonalization [9–11], and quantum Monte Carlo [12,13] methods, based on the t-J-type model. It was predicted that the single-particle spectrum consists of a sharp coherent peak, corresponding to a quasiparticle excitation, and an incoherent background. But this sharp coherent peak was not observed in the spectrum of electrons measured by angle-resolved photoemission spectroscopy on $Sr_2CuO_2Cl_2$ [14] and $Ca_2CuO_2Cl_2$ [15,16]. To reconcile the difference between theory and experiments, two kinds of scenarios were proposed to explain why the sharp quasiparticle peak is absent. One is to attribute this absence of sharp peak as an extrinsic effect induced by electron-phonon coupling [17]. The other regards this as an intrinsic effect resulting from a self-localization of doped holes in an AF background which smears out the coherent peak. From the self-consistent mean-field approximation, indeed it was found that the charge excitations are self-localized in a staggered AF ordered state [18–20]. This kind of charge self-localization was also predicted to exist in a single-hole Hubbard model by considering the nonperturbative phase string effect [21] or in the underdoped Mott insulator when the chemical potential lies within the pseudogap [22].

Recently local electronic structures in both doped and undoped Mott insulators were measured by STM [23,24]. In particular, the full electronic spectrum across the Mott-Hubbard gap and the spatially uniform Hubbard bands were observed in the recent STM study for the Mott insulator $Ca_2CuO_2Cl_2$ [24]. Moreover, a broad local in-gap state whose energy is below the upper Hubbard band was observed around a Cl defect on the surface of $Ca_2CuO_2Cl_2$, which is effectively a single electron doped Mott insulator [24].

To understand the STM experimental results, we calculate the local spectral function of electron for the Hubbard model without and with one electron doping on both square and triangular lattices using the cluster perturbation theory (CPT) [25,26]. We find that, apart from the Mott gap, a local in-gap state emerges below the upper Hubbard band. The total spectral weight of this in-gap state shows a rapid increase with the Hubbard interaction in a regime where the double occupation number of electrons shows a sharp reduction. Our result demonstrates that the in-gap state is an inherent feature of Mott insulators. For the one-band Hubbard model studied here, the spectral weights of the in-gap states come from both the upper and lower Hubbard bands, which shows a discrepancy with the experiments [24]. Based on the analysis of the three-band Hubbard model, we point out that the energy gap measured by the STM [24] is actually the gap between the upper Hubbard band and the charge transfer band of oxygen. Thus, the discrepancy in the spectral transfers is reconciled.

II. MODEL AND METHODS

The Hubbard model is defined by the Hamiltonian

$$H = -t \sum_{\langle i,j\rangle\sigma} c^{\dagger}_{i\sigma} c_{j\sigma} + U \sum_{i} n_{i\uparrow} n_{i\downarrow}, \tag{1}$$

where $c^{\dagger}_{i\sigma}$ is a creation operator of electron with spin σ on site i and $n_{i\sigma} = c^{\dagger}_{i\sigma} c_{i\sigma}$. $\langle i,j\rangle$ represents a pair of the nearest neighbor sites. The hopping constant t is set to 1 in the discussion below.

The CPT is based on the exact diagonalization of finite clusters and the intercluster coupling is taken as perturbation [25–33]. It can be used to treat a system with much larger

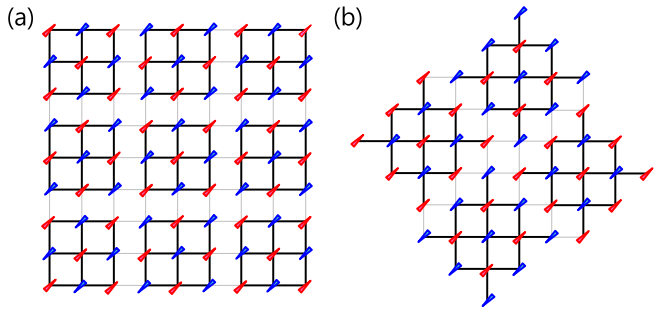

FIG. 1. (Color online) Tilings of the square lattice with (a) 9-site and (b) 13-site clusters. The triangles on the sites schematically illustrate the antiferromagnetic spin configuration.

lattice size than the exact diagonalization. In this method, the lattice is divided into a superlattice of decoupled clusters and each cluster contains N sites (as shown in Fig. 1 for example). In this superlattice, a lattice site is denoted by two indices (α,m), where α is the index of the cluster and m is the lattice coordinate. The Hamiltonian for the αth cluster H_α is first diagonalized using the Lanczos algorithm to obtain its ground-state energy E_0^α and the corresponding wave function $|\Omega^\alpha\rangle$. From this, the single-particle Green's function is calculated,

$$G''^{\alpha}_{m\sigma,m'\sigma'}(z) = \langle\Omega^\alpha|c^\alpha_{m\sigma}\frac{1}{z-H_\alpha+E_0^\alpha}c^{\alpha\dagger}_{m'\sigma'}|\Omega^\alpha\rangle + \langle\Omega^\alpha|c^{\alpha\dagger}_{m\sigma}\frac{1}{z-H_\alpha-E_0^\alpha}c^{\alpha}_{m'\sigma'}|\Omega^\alpha\rangle, \quad (2)$$

where z is a complex frequency.

The hopping between different clusters is taken as perturbation. We evaluate the local spectrum of the electron in real space. In this case, the Green's function for the whole system, which is a $2N_s \times 2N_s$ matrix with N_s the number of the whole lattice sites, can be expressed as

$$\mathbf{G}^{-1}_{\rm cpt}(z) = \mathbf{G}'^{-1}(z) - \mathbf{V}, \quad (3)$$

where the matrix elements of $\mathbf{G}'(z)$ and the intercluster hopping term $\mathbf{V}$ are defined by

$$G'_{\alpha m\sigma,\beta m'\sigma'}(z) = \delta_{\alpha\beta}G''^{\alpha}_{m\sigma,m'\sigma'}(z), \quad (4)$$

$$V_{\alpha m\sigma,\beta m'\sigma'} = -t\delta_{\alpha\neq\beta}\delta_{\langle\alpha m,\beta m'\rangle}\delta_{\sigma\sigma'}, \quad (5)$$

where $\langle\alpha m,\beta m'\rangle$ $(\alpha\neq\beta)$ means that (α,m) and (β,m') are two intercluster nearest-neighbor sites. The local density of states (LDOS) at site $i=(\alpha,m)$ is given by the imaginary part of the CPT Green's function,

$$A_i(\omega) = -\frac{1}{\pi}\lim_{\eta\to 0^+}\sum_\sigma \mathrm{Im}\, G_{{\rm cpt},i\sigma,i\sigma}(\omega-\mu+i\eta), \quad (6)$$

where μ is the chemical potential, and η is a broadening parameter which is used to smear out the finite-size effects. We determine its value by the average level spacing of the energy band in the noninteracting limit.

In our calculation, a standard $\eta=0.24$ is taken (calculations with η from 0.15 to 0.35 yield qualitatively the same results). The whole system contains 6×6 clusters. Periodic boundary conditions are assumed. The parent compound is at half-filling. The single electron is doped into one of the 36 clusters, which contains one more electron than other clusters and is denoted as the cluster γ. The results presented below are obtained with $U=10$ if not explicitly specified.

For the application of the method presented above, some care must be taken concerning the staggered ordering. On the square lattice, the ground state of the half-filled Hubbard model has the antiferromagnetic Neel order [1]. In our calculations, some cluster tilings, such as the 9-site and 13-site cluster tilings shown in Fig. 1, are not consistent with the Neel sublattice ordering if all clusters are treated identically. In the antiferromagnetic ordered state, the spin alignments are different between any two neighboring clusters in these cases. To reconcile with the long-range antiferromagnetic Neel order, we have swaped the spin orientation for any two nearest-neighbor clusters and taken the following transformation for the Green's functions obtained by the exact diagonalization: $G'_{m\sigma,m'\sigma'}=G_{m\sigma',m'\sigma}$.

III. RESULTS AND DISCUSSIONS

Figure 2 shows the results with the 12-site cross cluster tiling. By considering the symmetry of the cluster, we find that the sites with the same color shown in Fig. 2(a) are equivalent to each other and have identical spectra. Figure 2(b) shows the

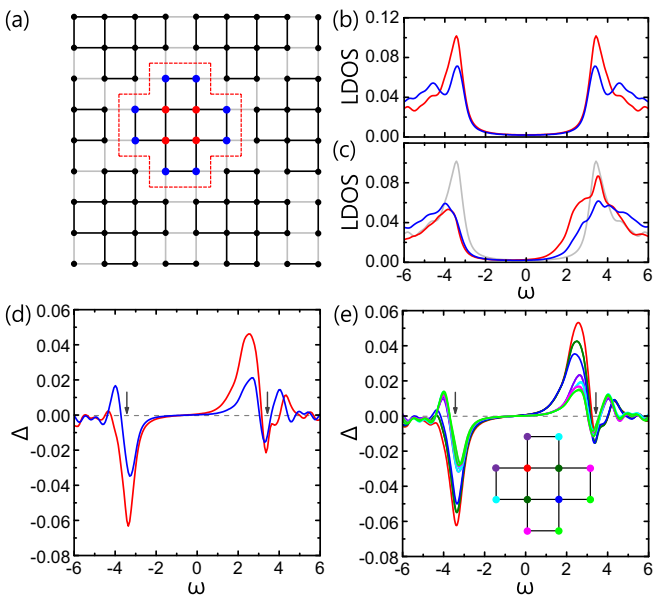

FIG. 2. (Color online) (a) A 12-site cluster, as enclosed by the red dashed lines, on the square lattice. The black and gray lines denote the intra- and intercluster hoppings, respectively. (b) and (c) The LDOS within the clusters without electron doping (i.e., at half-filling) and with one electron doping, respectively. The color lines indicate the results on the sites with the same colors in (a). The LDOS on the red sites in the undoped system is also shown with a gray line in (c) for comparison. (d) The difference Δ between the LDOS with and without electron doping on the corresponding color sites. (e) Δ on sites indicated by color dots in the inset with an on-site attractive potential $v=-0.08$ on the red site. The gray arrows in (d) and (e) indicate the peak positions of the LDOS for the lower and upper Hubbard bands on the red site at half-filling.

LDOS on the red and blue sites at half-filling. The LDOS does not distribute uniformly among the lattice sites within a cluster. This is an artifact of the approximation used in the CPT since the intra- and intercluster hoppings are treated differently in this theory. But the gap values between the lower and upper Hubbard bands, and the peak positions indicated by the gray arrows in Figs. 2(d) and 2(e) are the same on all sites within a cluster. This is because the on-site Hubbard interaction is treated rigorously in the CPT.

Now let us consider the case of one electron doping. Figure 2(c) shows the LDOS for the one-electron doped Hubbard model on the red and blue sites within the doped cluster [for comparison with the result shown in Fig. 2(b), the zero point of energy is rescaled to the middle of the Mott gap]. A broad in-gap state emerges below the upper Hubbard band on the central lattice sites within this doped cluster. The emergence of the in-gap state is accompanied by a reduction in the spectral weights of both the upper and lower Hubbard bands. Figure 2(d) shows the difference in the LDOS on the same lattice sites between the γ cluster and a cluster α which is far away from the γ cluster,

$$\Delta(\omega) = A_{\gamma m}(\omega) - A_{\alpha m}(\omega). \tag{7}$$

It shows clearly that the in-gap state results mainly from the spectral transfer from the lower Hubbard band. The weight of this broad in-gap state drops quickly on the site moving away from the center of the cluster, indicating that this in-gap state is highly localized around the doping center.

Because of the lattice symmetry, the four red sites have the same LDOS. To simulate the recent STM experimental result for $Ca_2CuO_2Cl_2$ with one Cl vacancy [24], we introduce a small attractive potential $v = -0.08$ to one of the four central sites in the γ cluster [i.e., the site in red in the inset of Fig. 2(e)]. As expected, the four central sites in this cluster are no longer equivalent to each other. The in-gap state is well localized around the site with an attractive potential. This is consistent with the experimental observation [24].

This localized feature of the in-gap state has also been found when several different cluster sizes and tilings are used on the square lattice. Figure 3 shows different cluster tilings, which consist of 8, 9, 12 (with rectangle shape other than cross shape), and 13 sites on each cluster (left panel), and the difference in the LDOS Δ on the corresponding sites (right panel). In all cases, the in-gap states emerge below the upper Hubbard band and are localized around the electron doping centers. Figure 4(a) shows the maximal height of the difference in the LDOS Δ for the in-gap states on different sites as a function of the distance R from the center of the doped cluster. We find that the in-gap states are basically localized and the results obtained on different cluster tilings show qualitatively similar behavior.

The result can be understood from the Hubbard model in the localized limit $U/t \to \infty$. In a N-site system at half-filling, the total spectral weights for both the lower and upper Hubbard bands are equal to N. Upon one-electron doping, the doped site is doubly occupied. This eliminates simultaneously one singly occupied state and one channel for adding an electron to a site which is already occupied. Thus the total spectral weights for both the lower and upper Hubbard bands are reduced by 1 and the missing spectral weight is transferred to the bottom of

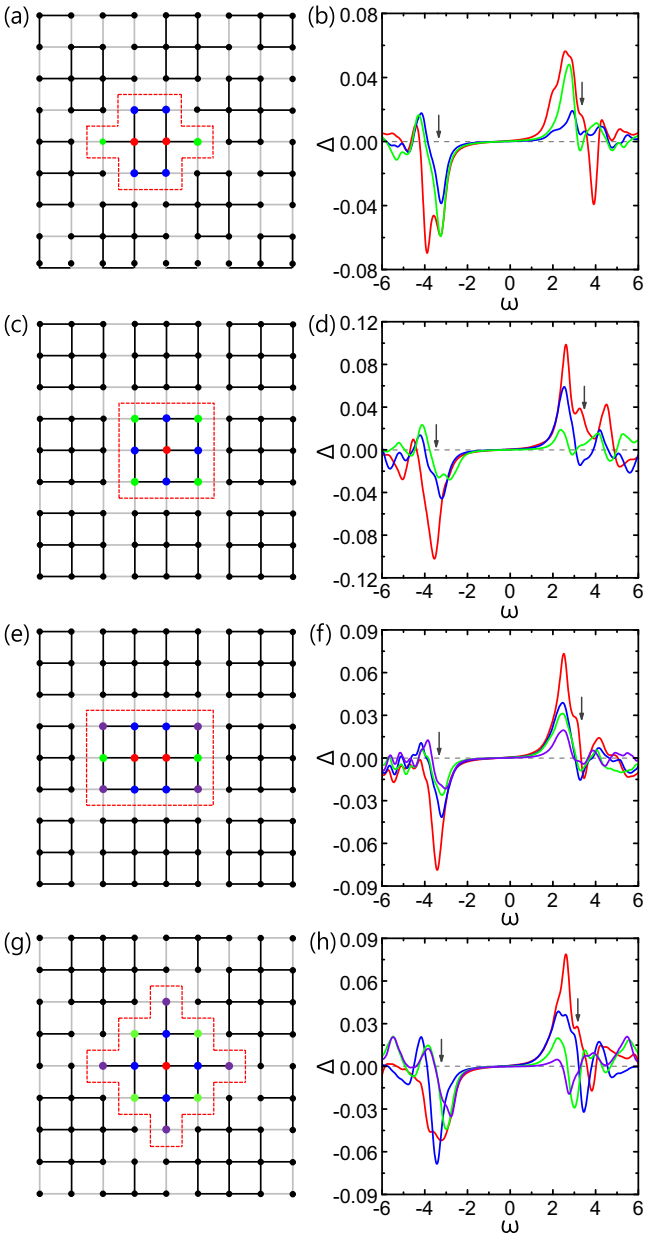

FIG. 3. (Color online) Left panel: Tilings of clusters with different sizes and shapes. (a), (c), (e), and (g) have respectively 8, 9, 12, and 13 sites in each cluster, as enclosed by the red dashed lines, on the square lattice. Right panel: Difference in the LDOS Δ on the corresponding colored sites in the left panel. The gray arrows indicate the peak positions in the LDOS for the lower and upper Hubbard bands without doping.

the upper Hubbard band just below the Fermi level [34–36], consistent with our calculation. In the STM measurement [24] on $Ca_2CuO_2Cl_2$, the spectral weight of the in-gap state seems to come mainly from the upper Hubbard band. To reconcile this discrepancy between our calculation and the experimental observation, we point out that the energy gap measured by the STM [24] is actually the gap between the upper Hubbard band and the charge transfer band of oxygen whose energy lies between the lower and upper bands, as illustrated by the green spectral weight in Fig. 4(b). Thus the transferred

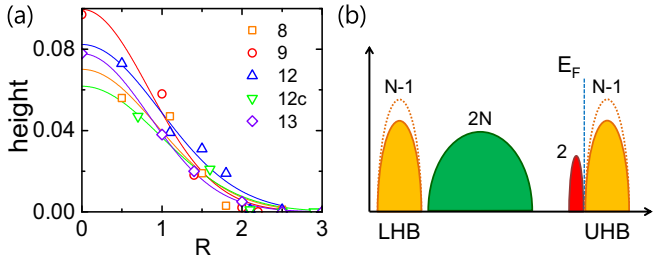

FIG. 4. (Color online) (a) Maximal height of the in-gap LDOS as a function of the distance R from the center of the doped cluster. The symbols with different colors represent the results obtained from different cluster tilings (the symbols denoted by 12c represent the results obtained with the 12-site cross cluster). The solid lines are the Gaussian fittings to the results. (b) Schematic diagram illustrating the spectral weight transfer in the localized limit in a single-electron doped three-band model. The green part between the lower (LHB) and upper (UHB) Hubbard bands represents the spectrum from the oxygen charge transfer band.

spectral weight in the lower Hubbard band, which lies well below the oxygen charge transfer band, is not observed by the STM.

Figure 5(a) shows the evolution of the difference in the LDOS Δ for the in-gap state on one of the red colored sites in Fig. 2(a) with U. From the result, we calculate the total spectral weight for the in-gap state defined by

$$W_{\rm loc} = \int_{\omega_1}^{\omega_2} \Delta(\omega)\, d\omega, \tag{8}$$

where ω_1 and ω_2 are the low and high energy boundary of LDOS within which $\Delta(\omega)$ is positive and $\Delta(\omega_1) = \Delta(\omega_2) = 0$. As shown in Fig. 5(b), $W_{\rm loc}$ increases rapidly with U, especially in the regime $2 < U < 6$, and then becomes nearly saturated above $U \sim 6$.

At half-filling, an important quantity characterizing the Mott physics is the double occupation of electrons. In order to quantify the correlation between the formation of the local in-gap state and the Mott physics, we calculate the double occupation number D defined by

$$D = \frac{1}{N_s} \sum_i \langle n_{i\uparrow} n_{i\downarrow} \rangle \tag{9}$$

at half filling. Figure 5(b) shows the double occupation number as a function of U. As expected, D is equal to 0.25 in the noninteracting limit $U \to 0$ and drops with increasing U. Although it approaches zero only in the limit $U \to \infty$, a rapid decrease occurs in the regime of $2 < U < 6$, it coincides with the regime in which $W_{\rm loc}$ increases rapidly. This suggests that the local in-gap state is an inherent feature of Mott insulators.

To further testify the above picture, we evaluate the total spectral weight for the in-gap state $W_{\rm loc}$ and the double occupation number D as a function of U for several different cluster sizes and tilings, and show the results in Figs. 5(c) and 5(d), respectively. The magnitude of $W_{\rm loc}$ varies with different clusters for large U, but it follows the same trend, especially in the regime $U < 6$. The double occupation numbers, obtained on three different clusters shown in Fig. 5(d), agree well with each other. These results suggest that the correlation between $W_{\rm loc}$ and D as depicted in Fig. 5(b) is indeed an intrinsic feature of the Hubbard model.

To explore the effect of lattice frustration on the in-gap state, we have also studied the single-electron doped Hubbard model on triangular lattices. A 13-site hexagram cluster tiling in a system containing 36 clusters with periodic boundary conditions is considered [Fig. 6(a)]. Figure 6(b) shows the difference in the LDOS on different sites. An in-gap state

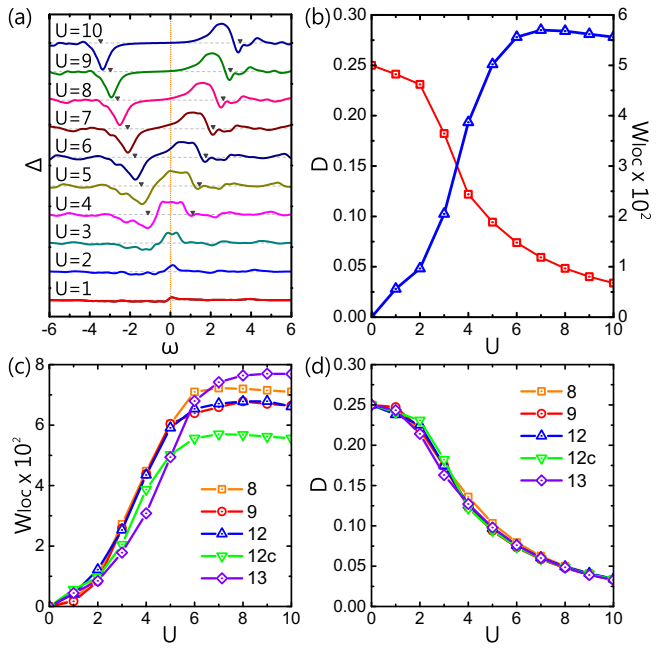

FIG. 5. (Color online) (a) Difference in the LDOS Δ on one of the red sites shown in Fig. 2(a) for different U. The peak positions of the LDOS for the lower and upper Hubbard bands at half-filling are indicated by the gray triangles. (b) U dependence of the double occupation number D (red line with squares) and the local spectral weight of the in-gap state $W_{\rm loc}$ (blue line with triangles). (c) and (d) $W_{\rm loc}$ and D as a function of U for several different cluster sizes and tilings (the symbols denoted by 12c represent the results obtained with the 12-site cross cluster).

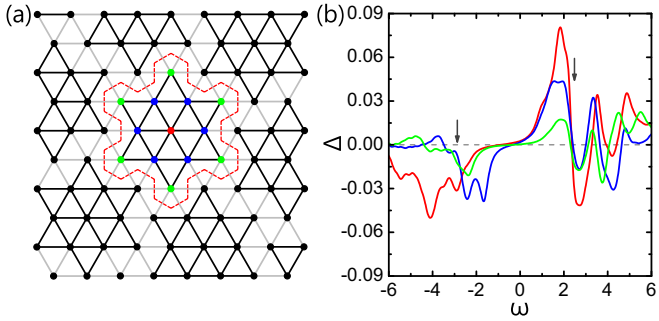

FIG. 6. (Color online) (a) A 13-site cluster, as enclosed by the red dash lines, on the triangular lattice. (b) The difference in the LDOS Δ on the sites with the same colors shown in (a). The peak positions in the LDOS for the lower and upper Hubbard bands at half-filling are indicated by the gray arrows.

below the upper Hubbard band (indicated by the right gray arrow) appears in the doped cluster and fades away from the doping center. This is similar to the result found on the square lattice and suggests that the local in-gap state is indeed a result of Coulomb repulsion.

IV. CONCLUSION

In summary, we calculate the local density of states for the Hubbard model at half-filling or with one electron doping on both square and triangular lattices using CPT. It is found that an in-gap state below the upper Hubbard band exists at and near the doping center irrespective of the lattice structure. The spectral weight of this in-gap state is inherently anticorrelated with the double occupation number of electrons, which is a key variable characterizing a Mott insulator, in the relevant physical parameter range. It indicates that the in-gap state is an inherent feature of Mott insulators. Our result gives a natural account for the STM experimental observation [24].

ACKNOWLEDGMENTS

This work was supported by the National Natural Science Foundation of China (Grants No. 11190024, No. 10934008, No. 11374138, No. 11204125, and No. 91021001) and by the National Basic Research Program of China (Grants No. 2011CB309703, No. 2011CB922101, and No. 2011CB605902).

[1] For a review, see P. A. Lee, N. Nagaosa, and X.-G. Wen, Rev. Mod. Phys. **78**, 17 (2006).
[2] P. W. Anderson, Science **235**, 1196 (1987).
[3] S. Schmitt-Rink, C. M. Varma, and A. E. Ruckenstein, Phys. Rev. Lett. **60**, 2793 (1988).
[4] C. L. Kane, P. A. Lee, and N. Read, Phys. Rev. B **39**, 6880 (1989).
[5] F. Marsiglio, A. E. Ruckenstein, S. Schmitt-Rink, and C. M. Varma, Phys. Rev. B **43**, 10882 (1991).
[6] G. Martinez and P. Horsch, Phys. Rev. B **44**, 317 (1991).
[7] J. Bała, A. M. Oleś, and J. Zaanen, Phys. Rev. B **52**, 4597 (1995).
[8] T. Xiang and J. M. Wheatley, Phys. Rev. B **54**, R12653 (1996).
[9] E. Dagotto, R. Joynt, A. Moreo, S. Bacci, and E. Gagliano, Phys. Rev. B **41**, 9049 (1990).
[10] Z. P. Liu and E. Manousakis, Phys. Rev. B **44**, 2414 (1991).
[11] P. W. Leung and R. J. Gooding, Phys. Rev. B **52**, R15711 (1995).
[12] E. Dagotto, A. Nazarenko, and M. Boninsegni, Phys. Rev. Lett. **73**, 728 (1994).
[13] T. K. Lee and C. T. Shih, Phys. Rev. B **55**, 5983 (1997).
[14] B. O. Wells, Z. X. Shen, A. Matsuura, D. M. King, M. A. Kastner, M. Greven, and R. J. Birgeneau, Phys. Rev. Lett. **74**, 964 (1995).
[15] F. Ronning, C. Kim, D. L. Feng, D. S. Marshall, A. G. Loeser, L. L. Miller, J. N. Eckstein, I. Bozovic, and Z. X. Shen, Science **282**, 2067 (1998).
[16] K. M. Shen, F. Ronning, D. H. Lu, W. S. Lee, N. J. C. Ingle, W. Meevasana, F. Baumberger, A. Damascelli, N. P. Armitage, L. L. Miller, Y. Kohsaka, M. Azuma, M. Takano, H. Takagi, and Z. X. Shen, Phys. Rev. Lett. **93**, 267002 (2004).
[17] A. S. Mishchenko and N. Nagaosa, Phys. Rev. Lett. **93**, 036402 (2004).
[18] W. P. Su, Phys. Rev. B **37**, 9904 (1988).
[19] J. A. Verges, E. Louis, P. S. Lomdahl, F. Guinea, and A. R. Bishop, Phys. Rev. B **43**, 6099 (1991).
[20] G. Seibold, E. Sigmund, and V. Hizhnyakov, Phys. Rev. B **57**, 6937 (1998).
[21] Z. Zhu, H.-C. Jiang, Y. Qi, C. Tian, and Z.-Y. Weng, Sci. Rep. **3**, 2586 (2013).
[22] T.-P. Choy and P. Phillips, Phys. Rev. Lett. **95**, 196405 (2005).
[23] For a review, see O. Fischer, M. Kugler, I. Maggio-Aprile, C. Berthod, and C. Renner, Rev. Mod. Phys. **79**, 353 (2007).
[24] C. Ye, P. Cai, R. Yu, X. D. Zhou, W. Ruan, Q. Q. Liu, C. Q. Jin, and Y. Y. Wang, Nat. Commun. **4**, 1365 (2013).
[25] D. Sénéchal, D. Perez, and M. Pioro-Ladrière, Phys. Rev. Lett. **84**, 522 (2000).
[26] D. Sénéchal, D. Perez, and D. Plouffe, Phys. Rev. B **66**, 075129 (2002).
[27] S. Pairault, D. Sénéchal, and A.-M. S. Tremblay, Phys. Rev. Lett. **80**, 5389 (1998).
[28] M. G. Zacher, R. Eder, E. Arrigoni, and W. Hanke, Phys. Rev. Lett. **85**, 2585 (2000).
[29] D. Sénéchal and A.-M. S. Tremblay, Phys. Rev. Lett. **92**, 126401 (2004).
[30] J. Kang, S. L. Yu, T. Xiang, and J. X. Li, Phys. Rev. B **84**, 064520 (2011).
[31] S. L. Yu, X. C. Xie, and J. X. Li, Phys. Rev. Lett. **107**, 010401 (2011).
[32] S. L. Yu and J. X. Li, Phys. Rev. B **85**, 144402 (2012).
[33] M. Potthoff, M. Aichhorn, and C. Dahnken, Phys. Rev. Lett. **91**, 206402 (2003).
[34] H. Eskes, M. B. J. Meinders, and G. A. Sawatzky, Phys. Rev. Lett. **67**, 1035 (1991).
[35] M. B. J. Meinders, H. Eskes, and G. A. Sawatzky, Phys. Rev. B **48**, 3916 (1993).
[36] L. F. Feiner, Phys. Rev. B **48**, 16857 (1993).